CUP – a new high-flux irradiation position at the ANITA neutron facility at TSL

Alexander V. Prokofiev, *Member, IEEE*, Elke Passoth, Anders Hjalmarsson, and Mitja Majerle

***Abstract*—A new irradiation position has been constructed, characterized, and put into operation at the ANITA facility in The Svedberg Laboratory (TSL) for accelerated testing of components and systems for single event effects. Results of beam characterization measurements are reported. The energy-integrated neutron flux above 10 MeV, amounting to more than 10^7 $cm^{-2}·s^{-1}$, is the highest among the facilities with atmospheric-like spectra. The employed characterization and simulation techniques are applicable for a broad class of neutron facilities.**

***Index Terms*—accelerated testing, integrated circuit radiation effects, neutron beams, neutron detectors, neutron radiation effects, radiation facilities, single event effects, soft error rates, terrestrial radiation environments, test facilities.**

I. Introduction

The increasing complexity of electronic components and systems, together with strengthening requirements for stable operation of critical infrastructures, emphasizes the importance of reliability testing. One of the major reliability concerns comes from single-event effects (SEE) caused by directly and indirectly ionizing radiation [1].

High-energy neutrons, produced by cosmic rays in the Earth's atmosphere, may cause a significant or dominating fraction of the soft error rate (SER) in components and systems at aircraft altitudes as well as in terrestrial environments [2, 3]. Guidelines for neutron SER (nSER) testing can be found in recent standards [4, 5]. Accelerated nSER testing is mostly performed at spallation facilities [6-9] that produce neutrons with "white" spectra, which resemble the spectrum of neutrons in the atmosphere and in terrestrial environments. This resemblance allows one easily to deduce the failure-in-time (FIT) rate for a device under test (DUT).

One of the recent trends in nSER testing is a growing need in more intense fields of high-energy neutrons, which would allow one to observe less frequent events and to get reasonable event rates, thus making it possible to accumulate sufficient statistics of events in shorter times. The trend, especially clear for DUTs with very low FIT rates, is corroborated by our observations at the ANITA facility (*A*tmospheric-like *N*eutrons from th*I*ck *TA*rget) [9] in The Svedberg Laboratory (TSL), namely: (1) a dominant fraction of the nSER-testing beam time is spent with the highest possible flux (despite the possibility to control and adjust it); (2) in certain cases, the available neutron flux is still insufficient, and the users are forced to switch to proton beams, for which the available flux is higher; (3) the facility has been receiving explicit users' requests for neutron flux enhanced by *an order of magnitude* compared to the standard ANITA configuration [9].

The outlined need is addressed in the present work, aimed at development of a new irradiation position, further referred to as the *Close User Position (CUP)*, at the ANITA facility.

A. V. Prokofiev is with the The Svedberg Laboratory (TSL) and the Department of Physics and Astronomy, Uppsala University, Box 533, 751 21 Uppsala, Sweden (e-mail: alexander.prokofiev@physics.uu.se).

E. Passoth is with The Svedberg Laboratory, Uppsala University, Box 533, 751 21 Uppsala, Sweden (e-mail: elke.passoth@tsl.uu.se).

Anders Hjalmarsson is with the Department of Physics and Astronomy, Uppsala University, Box 515, 751 20 Uppsala, Sweden (e-mail: anders.hjalmarsson@physics.uu.se).

Mitja Majerle is with the Nuclear Physics Institute of ASCR, Rež near Prague, Czech Republic (e-mail: majerle@ujf.cas.cz).

II. Description of The Facility

The description of the ANITA facility, prior to the present upgrade, is given in [9] and briefly recapitulated in Sect. II-A. The newly developed CUP facility is presented in Sect. II-B.

A. The conventional ANITA facility

A layout of the facility is presented in Fig. 1. The proton beam, accelerated to ≈180 MeV energy, arrives at a 2.4-cm thick, water-cooled tungsten target, further referred to as the *production target*, which fully stops the incident protons. Neutrons are created in nuclear interactions between incident protons and tungsten nuclei in the production target. The production target is situated inside a massive bending magnet in a concrete cave, for enhanced shielding of surrounding areas. The cave and the conventional user area are separated by a 1-m thick iron frontal wall (see Fig. 1) with a selectable collimator aperture that defines the size and the shape of the neutron beam spot. Positions available for DUT are located at distances ranging from 250 cm to ~15 m, thus allowing further variation of the beam size and flux. (Here and further in the text, the distances are given from the center of the production target, along the beam axis). The neutron beam monitoring is provided by thin-film breakdown counters (TFBC) [10-12], by a fission ionization chamber, as well as by proton current measurements on the production target. The highest flux in the conventional user area is available at the *Standard User Position (SUP)*, located at the distance of 250 cm. The energy-integrated flux above 10 MeV amounts to 10^6 $cm^{-2}·s^{-1}$ for the *standard ANITA-SUP neutron field*, which originates from incident proton beam with current of 215 nA, adopted as a facility standard during recent years. The facility is frequently used for nSER studies and testing, see e.g. [13-16], studies of ageing effects in image sensors [17], development/calibration

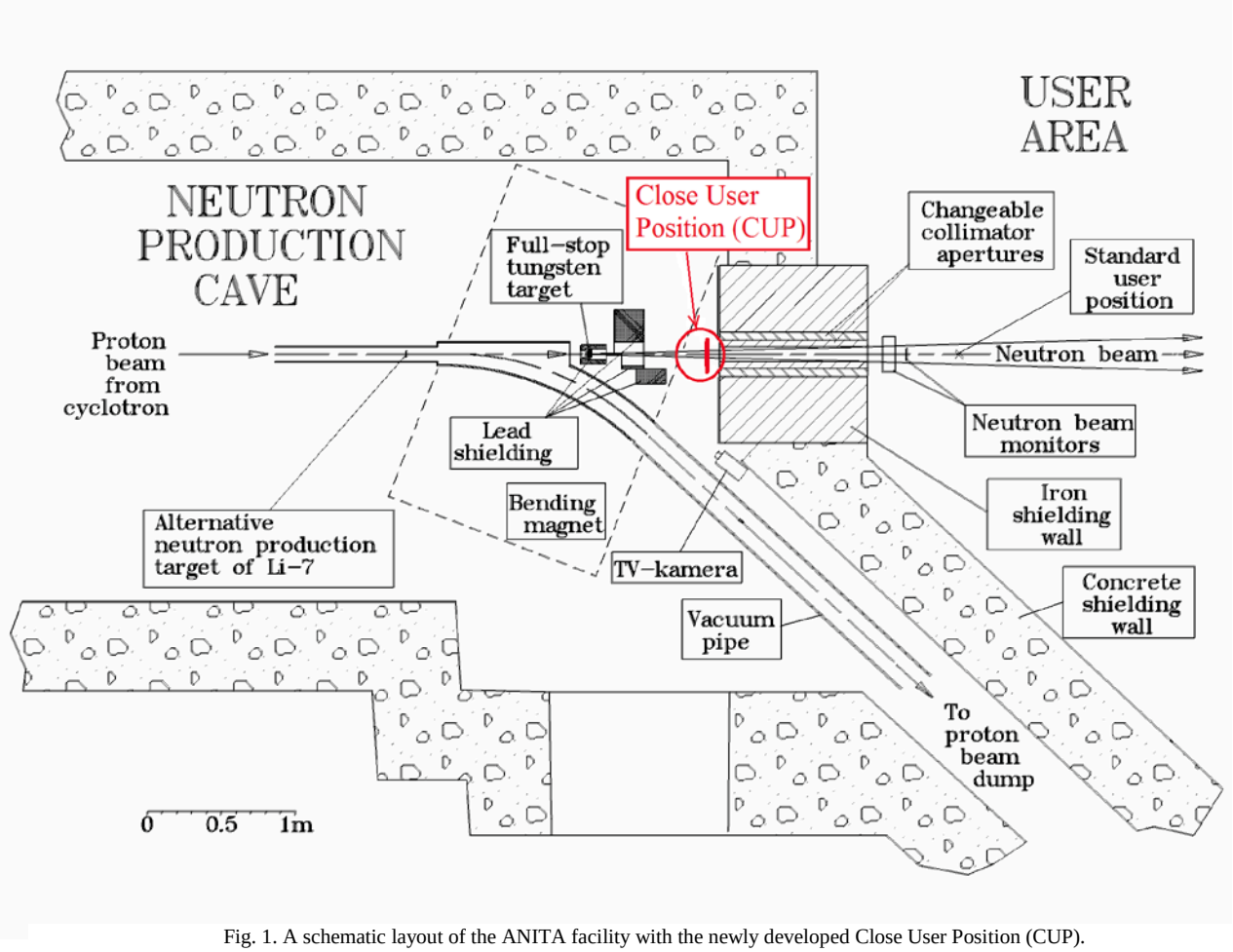

Fig. 1. A schematic layout of the ANITA facility with the newly developed Close User Position (CUP).

of neutron monitors [18-22], etc.

B. *The ANITA-CUP facility*

The irradiation position at the ANITA-CUP facility, further referred to as the *in-beam position*, is located in the cave, between the bending magnet and the frontal wall (see Figs. 1 and 2). The center of the in-beam position is located at the distance of 75 cm downstream of the production target and 160 cm below the cave roof level. A vertical access shaft (see Fig. 3), equipped with a rail and a pulley system, connects the in-beam position to the *loading position*, located at ~1.5 m above the roof of the cave. The loading position can be accessed by the user for mounting the DUT and associated equipment (see Sect. VI for more details). The DUT, mounted on a trolley sled (see Fig. 3), can be moved along the rail and lowered to the in-beam position. An additional rail in the shaft is intended for a neutron monitor, which can be placed downstream of the DUT.

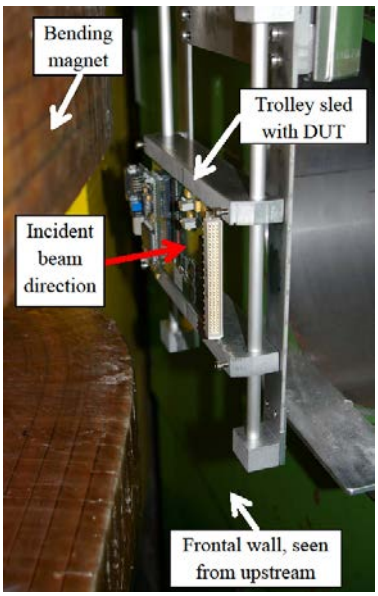

Fig. 2. A DUT at the in-beam position of the CUP facility.

A user may perform irradiations at the CUP simultaneously with the ones at the conventional user area. (Here and further in the text, “at the CUP” means “at the in-beam position of the CUP facility”). Using neutron monitor data, one can account for (usually minor) attenuation of the neutron beam caused by the DUT installed at the CUP.

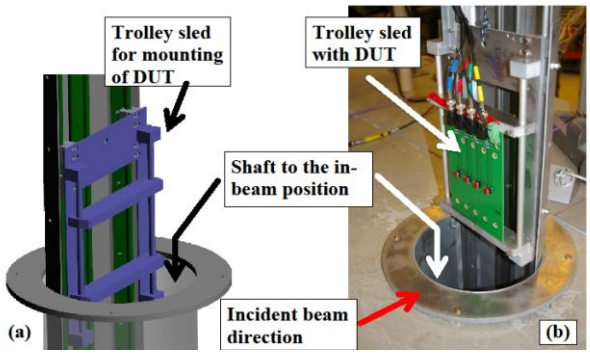

Fig. 3. (a) The trolley sled for mounting of the DUT. (b) The DUT in its way from the loading position to the in-beam position.

An irradiation position similar to the CUP is available at the TRIUMF neutron facility [7]. A brief comparison is presented in Sect. V.

III. Neutron Field Simulations

A. The geometrical input

The simulation geometry included the target arrangement, the cooling water, the shielding constructions in the target area, the magnet poles, and the frontal wall with the collimator aperture (see Fig. 1). This level of detailing is considered sufficient for simulation of the high-energy part of the neutron field (above 1 MeV), which is of primary importance for nSER testing. The simulation did not aim at reproducing experimental data on the thermal neutron component, presented in Sect. IV-D.

We have simulated neutron fields at the SUP as well as at a few selected locations in the CUP area, with different collimator openings. A selection of the CUP results, reported below, includes simulations at two locations: (1) at the in-beam position; (2) at the distance of 84 cm downstream of the production target. The latter location is further referred to as the *CUP-ToF position*, or briefly the *CUP-ToF*, because it has been utilized for a time-of-flight (ToF) measurement of a neutron-induced fission spectrum, as reported in Sect. IV-A.

B. The MCNPX code

The simulations have been performed with the MCNPX code [23, 24], version 2.7.0. MCNPX is a general-purpose three-dimensional Monte Carlo radiation transport code for modeling the interaction of radiation with matter. MCNPX is used in accelerator applications, nuclear medicine, nuclear safeguards, homeland security, and much more.

For modeling of interactions of nucleons with energy up to 150 MeV with materials (in our application, with the neutron production target and surroundings), the MCNPX code utilizes the LA150 data libraries [25]. For energies above 150 MeV, where tabular data are not available, the user has to choose one of several physics models incorporated in the code. The simulation in the present work has been performed using the Cascade-Exciton Model (CEM) [26], version CEM03. The other available models (Bertini, INCL, ISABEL) have been tried as well; the differences in the simulated results are barely seen and appear only at the highest neutron energies, where the spectral fluence is low. It is therefore unlikely that the choice of the model in MCNPX plays a critical role in the present application.

C. Simulation results

Simulated results for the standard ANITA-SUP field have been found similar to the ones presented in [9]. Simulated spectral neutron fluence data at the CUP-ToF are shown in Fig. 4 on a lethargy plot, for which equal areas under the fluence curve represent equal values of energy-integrated fluence [4]. This facilitates comparisons and judgments on the importance of different energy ranges in spectra spanning over many decades in energy. The data are presented for three

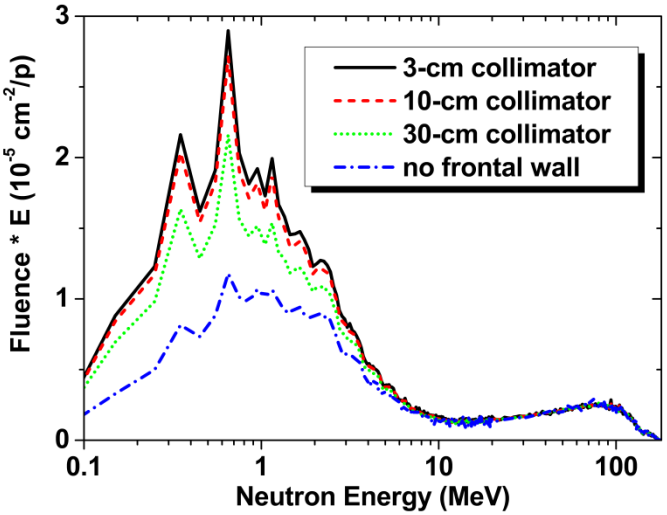

Fig. 4. Simulated spectral fluence data at the CUP-ToF position, in the lethargy scale, per incident proton on the production target. The black solid line, the red dashed line, and the green dotted line represent the results for different collimator apertures, with diameter 3, 10.2, and 30 cm, respectively. The blue dash-dotted line represents the results obtained for an imaginary geometrical case, in which the frontal wall is completely removed.

different collimator apertures, as well as for an imaginary geometrical case, in which the frontal wall is completely removed. The four presented datasets are indiscernible at energies above ~10 MeV. At lower energies, the spectral fluence increases with the decrease of the collimator aperture diameter. Among collimators with diameters ≤10.2 cm, the data are similar within ±3%, including also data for another imaginary case of the completely closed frontal wall (not shown in Fig. 4). One can conclude that the neutron field in the CUP area has a component originating from the frontal wall, as discussed further in Sect. III-E.

D. Spectral fluence parameterization

Simulation results reported below have been renormalized in such a way that the energy-integrated flux above 10 MeV is retained for the standard ANITA-SUP field characterized in [9]. That benchmark was independently confirmed in the same work by measurements correlated to the LANSCE ICE House facility [6].

After the renormalization, the spectral fluence $\Phi(E)$ per incident proton on the production target, at the CUP in-beam position, with 10.2-cm collimator, has been parameterized versus neutron energy E as a function similar to the one suggested in [9]:

$$\Phi(E) = \frac{1}{E}\sum_{i=1}^{2} g_i \varphi_i \ , \qquad (1)$$

where

$$\varphi_i = \begin{cases} q_i\,(E/E_{0i})^{p_i}\,, \text{ if } 0 < E \le E_{1i} \ , \\ exp\left[-\frac{ln^2\,(E/E_{0i})}{2\,\Delta_i^2}\right] \ , \text{ if } E_{1i} \le E < E_{max} \\ 0, \text{ if } E > E_{max} \ , \end{cases} \qquad (2)$$

$$q_i = \left(\frac{E_{1i}}{E_{0i}}\right)^{-p_i} \exp\left(-\frac{ln^2\frac{E_{1i}}{E_{0i}}}{2\Delta_i^2}\right), \quad (3)$$

E_{max} = 175 MeV, and g_i, E_{0i}, E_{1i}, Δ_i, and p_i are fitting parameters given in Table I.

TABLE I.
THE FITTING PARAMETERS IN THE PARAMETERIZATION OF THE SPECTRAL NEUTRON FLUENCE AT THE IN-BEAM POSITION OF THE CUP FACILITY, WITH 10.2-CM COLLIMATOR

i	g_i (cm^{-2})	E_{0i} (MeV)	E_{1i} (MeV)	Δ_i (*no-dim*)	p_i (*no-dim*)
1	4.985×10^{-6}	79.74	73.06	0.3623	0.6614
2	3.040×10^{-5}	0.7064	0.3480	1.1058	1.0076

The resulting parameterization is shown in Fig. 5a. A similar spectral fluence parameterization for the CUP-ToF is shown in Fig. 5b on a lethargy plot.

E. Multicomponent model of the CUP neutron field

We have compared the simulated spectral fluence data at the CUP-ToF and at the SUP with 10.2-cm collimator. The latter data, re-normalized to the CUP-ToF according to the $1/R^2$ law, have been found indiscernible from the CUP-ToF data within the uncertainty limits at energies above ~60 MeV. Thus, the high-energy component of the CUP-ToF neutron field has properties (spectrum, fluence per unit solid angle) that are similar to the ones of the field at the SUP, which is shielded by the frontal wall against neutrons produced in surroundings at the cave. It is natural therefore to interpret the high-energy component of the CUP-ToF field as the one comprising neutrons that come directly from the production target.

The observations made in the context of Figs. 4 and 5b have allowed us to consider the neutron field at the CUP-ToF as a sum of the following three components (see the legend in Fig. 5b):

1) The Direct Component (DC), comprising neutrons that originate from the production target, propagate at angles near 0° relative to the primary beam direction, and reach the location of interest without having interacted with other objects' materials. The DC is collimator-independent and can be estimated from the SUP field. As seen in Fig. 5b, the DC dominates the CUP-ToF field at the highest energies and down to a few MeV.

2) The Frontal Wall Component (FWC), originating from neutron scattering, moderation, and secondary neutron production in the frontal wall. Due to aperture limitations caused by production target surroundings, only the central part of the wall is an effective FWC source. The FWC is collimator-dependent and can be estimated as the difference between the spectral fluence for the given collimator case and for the imaginary "no-wall" case (see Fig. 4). As seen in Fig. 5b, the FWC reaches maximum (in the lethargy scale) at ~0.5 MeV and vanishes out at ~10 MeV. The lack of high-energy neutrons in the FWC is understandable, because the CUP area is "seen" from the frontal wall at backward angles, for which high-energy neutron emission is suppressed.

3) The Surroundings Component (SC), which is collimator-independent and can be interpreted as a result of neutron interactions in the CUP surroundings, except the production target and the frontal wall. Similar to the FWC, the SC is dominated by sub-MeV neutrons, but stretches up to energies of ~60 MeV.

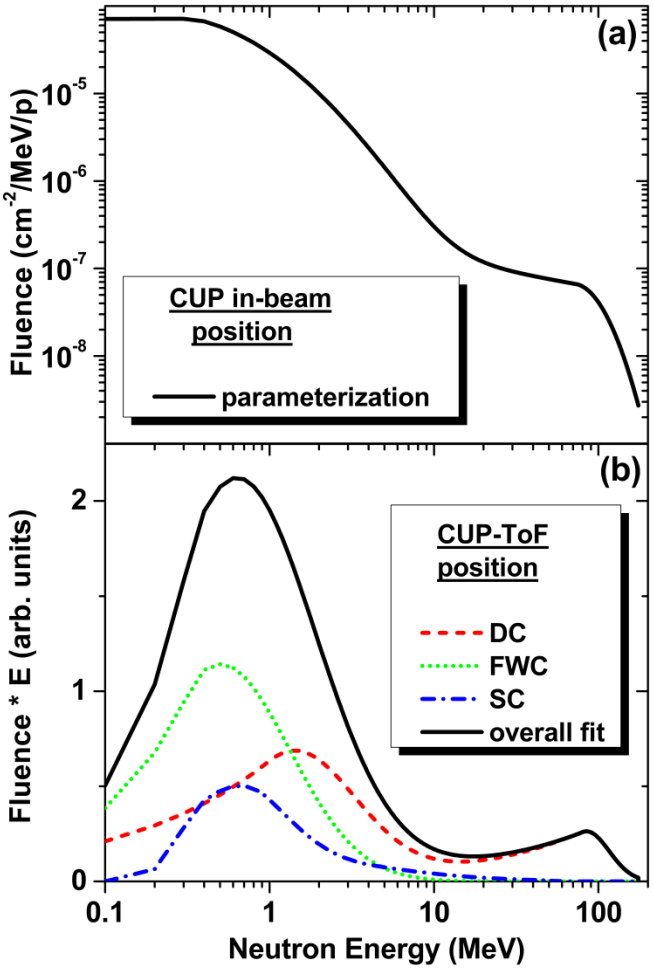

Fig. 5. The simulated spectral neutron fluence per incident proton on the production target, versus neutron energy: *(a)* at the CUP in-beam position, with the 10.2-cm collimator. The line represents the parameterization given in Table I; *(b)* at the CUP-ToF position, with the 3-cm collimator, in the lethargy scale. The three components in the neutron field are represented by the red dashed line (Direct Component, DC), the green dotted line (Frontal Wall Component, FWC) and the blue dash-dotted line (Surroundings Component, SC). The black line is the sum of the three components, representing the overall spectral fluence.

Neither FWC nor SC give significant contributions to the SUP neutron field, due to the presence of the frontal wall that shields the conventional user area from neutrons propagating at skewed angles.

The formulated semi-empirical multicomponent neutron field model has been found useful for interpretation of experimental characterization data, as described in Sect. IV.

IV. CHARACTERIZATION OF ANITA-CUP NEUTRON FIELD

The neutron field at the CUP area has been experimentally characterized with regard to the neutron spectrum (Sect. IV-A), the energy-integrated neutron flux and 1-MeV equivalent flux (Sect. IV-B), the spatial profiles (Sect. IV-C), thermal neutrons (Sect. IV-D), and γ-rays (Sect. IV-E).

A. *ToF studies of the neutron spectrum at the CUP*

1) *Experiment*

We have measured a ToF spectrum of neutron-induced fission events in an isotopically-pure ^{238}U target. The measurement has been performed at the CUP-ToF, with 3-cm collimator, using a TFBC for detection of fission fragments. The measured time is an interval elapsed from the arrival of a proton burst at the production target until the detection of a fission event at the CUP-ToF. Further details of the method are described in [9, 11, 12]. The measurement provided only relative ToF scale, i.e. the primary ToF data were arbitrarily shifted along the time axis. The magnitude of the shift has been determined, and thus the absolute ToF scale has been established, by comparison of the experimental data to simulated ones, described in Sect. IV-A2. The final experimental spectrum of fission events is shown in Fig. 6 by symbols.

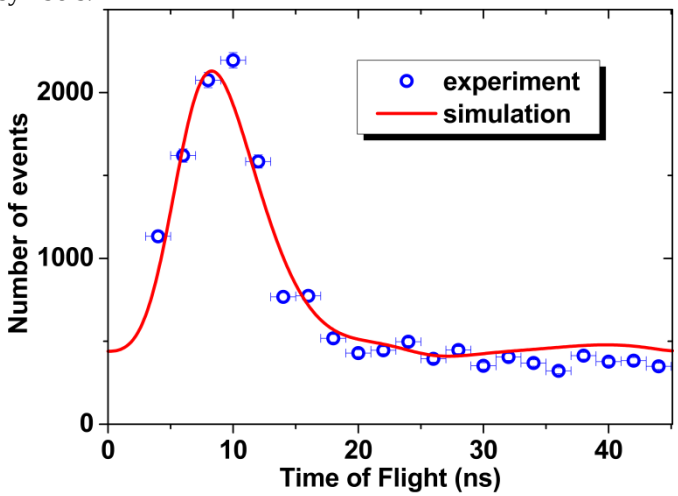

Fig. 6. Experimental (symbols) and simulated (line) ToF spectra of fission events in a ^{238}U target at the CUP-ToF position. The error bars indicate statistical uncertainties and the ToF bin width.

2) *Simulation*

The ToF spectrum of ^{238}U fission events has been simulated for the geometrical case that was employed in the respective experiment (see Sect. IV-A1). In order to be able to reproduce the experimental spectrum, it has been found necessary to employ the multicomponent model of the CUP neutron field, outlined in Sect. III-E. The spectral fluence data for each component, shown in Fig. 5b, have been folded with the standard ^{238}U(n,f) cross section [27], thus resulting in distributions of fission events over neutron energy. Next processing step, relativistic energy-to-ToF conversion, had to be made individually for each component, as outlined below.

(i) **For DC neutrons**, the flight path length was assumed to be constant and equal to the distance from the production target to the CUP-ToF. Therefore, the distribution of DC-induced fissions could be straightforwardly converted from the energy scale to the ToF one.

(ii) **For a FWC neutron**, overall ToF is a sum of two contributions, t_1 and t_2, where t_1 is ToF of a primary neutron in its path from the production target to the interaction point in the wall, and t_2 is ToF of a secondary neutron in its path from the wall to the CUP-ToF. t_1 and t_2 depend on respective neutron energy and flight path length. Consequently, t_1 and t_2 are not constant but can be represented by distributions, determined under the following simplifying assumptions: (1) only interaction points located near the upstream surface of the wall give significant contribution to the FWC; (2) the effective incident neutron spectrum on the wall is represented by the component with i=1 in Eq. (1); (3) the length of the path from the wall to the CUP-ToF has been assumed constant and has been determined by averaging path lengths originating from different locations over the irradiated area of the wall. Finally, the overall ToF distribution of FWC-induced fissions has been calculated by convolution of t_1 and t_2 distributions.

(iii) **SC neutrons** originate from objects that are widely distributed over the cave. Consequently, there is no single specific path for SC-neutrons propagating to the CUP. Moreover, the SC is dominated by low-energy neutrons (see Sect. III-E), for which the flight times spent on paths from surroundings to the CUP are comparable to, or even longer than the proton burst repetition period. As a consequence, the SC must give a smeared-out, structureless contribution to the fission ToF spectrum. Therefore we have assumed that the distribution of SC-induced fissions is time-uncorrelated and uniform over the burst repetition period.

The remaining processing steps comprised summation of the fission ToF spectra coming from the three components, correction for frame overlap, broadening the spectrum due to the limited time resolution in the measurement system and in the incident proton beam, and finally normalization of the simulated spectrum to the number of the experimentally observed fission events. The final simulated spectrum is shown in Fig. 6 as a line.

3) *Discussion*

As seen in Fig. 6, the fission ToF spectrum is dominated by a prominent peak at ToF ≈ 8 ns, which corresponds to the (relatively weak) high-energy peak at ~80 MeV in Fig. 5b. Contrary to that, the intense low-energy peak in the neutron spectrum does not result in any structure in the fission ToF spectrum. We interpret it as a result of the following factors: (1) low-energy neutrons are de-favourized by the ^{238}U(n,f) reaction with the threshold at ~1 MeV; (2) SC-induced fissions, which give a significant contribution to the low-energy peak, are time-uncorrelated; (3) FWC-induced fissions, which give the largest contribution to the low-energy peak, result from interactions in the frontal wall that are preferentially caused by high-energy neutrons. Consequently, *many fission events induced by low-energy neutrons bear ToFs that are characteristic for high-energy neutrons*.

The achieved degree of agreement between the experiment and the simulation allows us to conclude that the adopted multicomponent model provides a realistic description of the neutron field in the CUP area. More sophisticated Monte Carlo calculations, including, in particular, treatment of neutron transport time, would be needed in order to reproduce the experimental ToF spectrum with further improved fidelity.

On the other hand, improved treatment of the timing aspects would not influence the overall simulated spectral fluence data reported in Sect. III.

B. Fission rate and energy-integrated flux characteristics

In order to characterize the energy-integrated neutron flux at the CUP, we have measured the integral count rate of neutron-induced fission events, further referred to as the *fission rate*, in a ^{238}U target. A TFBC with the target has been exposed alternately at the CUP in-beam position and at the SUP, in both cases with 10.2-cm collimator. Data from other neutron monitors (see Sect. II-A) have been utilized for normalization of the exposures. The experimentally determined ratio of the normalized fission rates at the CUP and the SUP has amounted to 14.8 ± 0.9. The same quantity has been deduced from the simulations of the spectral neutron fluence at the CUP and the SUP (see Sect. III), folded with the standard ^{238}U(n,f) cross section data [27]. The calculated ratio amounts to 14.0. Thus, the experimental and calculated results agree within the uncertainty limits and deviate significantly from the value 11.1, which stems from a plain $1/R^2$-law calculation. Obviously, the deviation is due to FWC and SC neutrons (see Sect. III-E), which are present at the CUP area but absent at the SUP.

In Table II, integrated characteristics are presented for the *standard ANITA-CUP neutron field*, defined as the one at the CUP in-beam position, created by incident proton beam with the standard current of 215 nA, in the presence of 10.2-cm collimator.

TABLE II.
INTEGRATED CHARACTERISTICS OF THE STANDARD CUP NEUTRON FIELD

Characteristics	Value	Unit
Energy-integrated flux >10 MeV	1.17×10^{7}	$cm^{-2}\cdot s^{-1}$
Energy-integrated flux >1 MeV	5.5×10^{7}	$cm^{-2}\cdot s^{-1}$
Energy-integrated flux >0.1 MeV	1.2×10^{8}	$cm^{-2}\cdot s^{-1}$
1-MeV equivalent neutron flux	1.15×10^{8}	$cm^{-2}\cdot s^{-1}$
Acceleration factor	3.2×10^{9}	-

The values of energy-integrated flux above 10 MeV, 1 MeV, and 0.1 MeV have been obtained by integration of the parameterized fluence data given in Table I. The acceleration factor is the ratio of the energy-integrated flux above 10 MeV at the ANITA-CUP and in the standard terrestrial neutron field [4]. A comparison of the integrated flux above 10 MeV to the one in the standard ANITA-SUP field gives the factor 11.7, which shows only 5% excess of the flux at the CUP over the plain $1/R^2$-law-based value. This proximity reflects the fact that the CUP spectrum above 10 MeV is dominated by the DC (see Sect. III-E), which indeed follows the $1/R^2$ law.

The 1-MeV equivalent neutron flux [28] has been determined by folding the fluence parameterization (see Table I) with damage-function data for silicon, taken from [28, 29].

Similarly to the conventional user area, the flux at the CUP is controllable by the user [9].

C. Beam profiles and geometrical limitations at the CUP

Spatial profiles of the neutron beam, measured using a movable TFBC with a ^{238}U target, are shown in Fig. 7. The data are presented for both the profiles, vertical and horizontal. The neutron field has been found to be uniform within ±10% in the central area of the beam, 20 cm × 20 cm. The limitations in the vertical direction, shown as dashed lines in Fig. 7, are due to the aperture of the bending magnet upstream of the CUP.

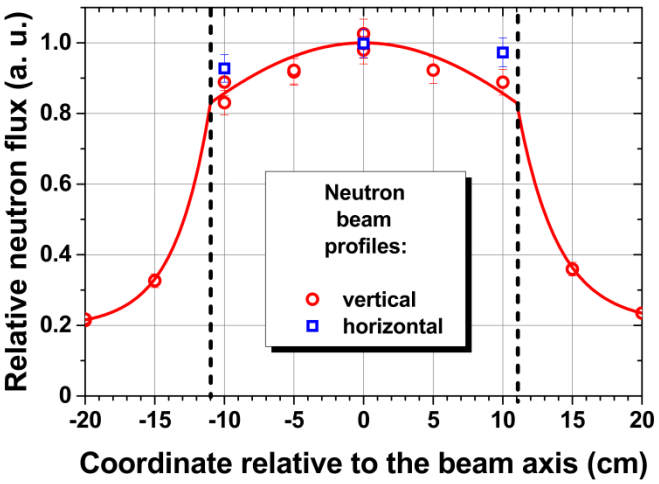

Fig. 7. The neutron beam profiles at the CUP. Symbols (red circles and blue squares) represent experimental results for the vertical and horizontal profile, respectively. The solid red line is to guide the eye through the experimental data for the vertical profile. The dashed lines show limitations in the vertical direction due to the aperture of the bending magnet upstream of the CUP.

In the horizontal direction, the usable width of the neutron beam is limited by the dimensions of the shaft and the trolley sled (see Sect. II-B). The maximum overall dimensions of the DUT that can be accommodated are specified in Sect. VI.

D. Thermal neutrons at the CUP

Thermal neutrons have been observed at the CUP, using a TFBC with a ^{235}U target. The normalized fission rates have been compared for two irradiations of the same detector arrangement, with and without cadmium shielding. After normalization to the standard ANITA-CUP neutron field, the thermal neutron flux amounted to 2.3×10^{6} $cm^{-2}\cdot s^{-1}$, or 20% relative to the energy-integrated flux above 10 MeV.

Thermal neutrons in the field may need to be shielded against, either to exclude thermal neutron effects or to discriminate between effects due to thermal and fast neutrons [4, 30]. The shielding can be achieved by sheets of materials containing boron or cadmium. Already a 1-mm thick cadmium metal sheet provides sufficient suppression of the thermal neutron flux.

E. γ-rays at the CUP

The dose rate from prompt γ-rays at the CUP, measured with a conventional radiation survey instrument, has been found to be proportional to the beam current on the production target. For the standard ANITA-CUP neutron field, the dose rate amounts to ≈17 rad/h. This result is considered as an upper limit, because it may include a contribution from secondary charged particles originating from neutron interactions with materials in the survey instrument.

V. Comparisons with Other Facilities. Spectrum Fidelity

In Fig. 8, the spectral flux for the standard ANITA-CUP neutron field is shown in comparison with data for ANITA-SUP at TSL [9], ICE House facility at LANSCE [6], TRIUMF neutron facility [7], ISIS VESUVIO [8], and the reference terrestrial neutron field [4]. As seen in Fig. 8, the ANITA-CUP neutron flux in the energy range up to 150 MeV is *at least* a few times higher than at the other facilities.

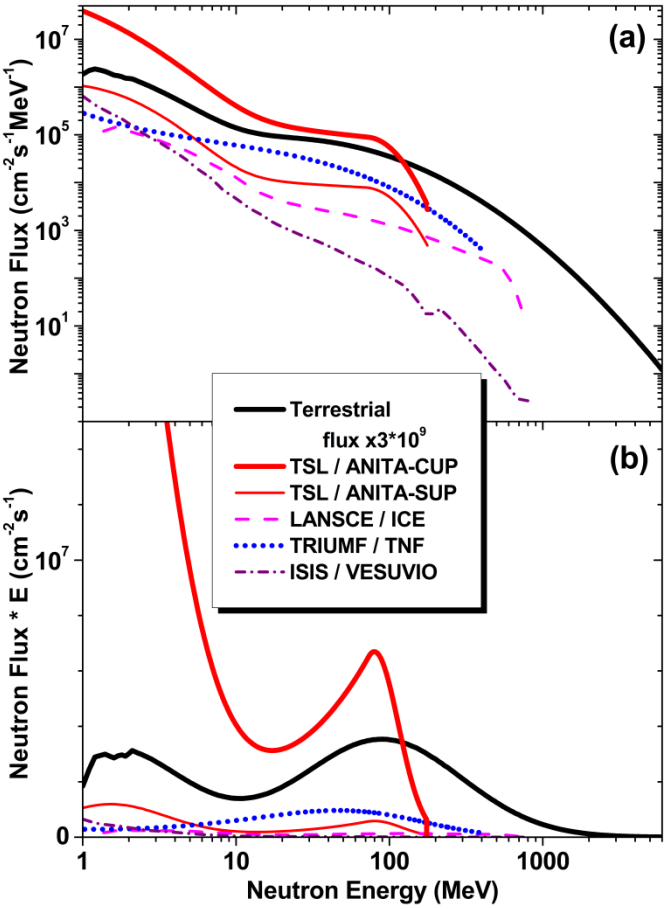

Fig. 8. (*a*) The spectral flux for the standard ANITA-CUP neutron field (red thick solid line), in comparison with the ANITA-SUP [9] (red thin solid line), the LANSCE ICE House facility [6] (magenta dashed line), the TRIUMF neutron facility [7] (blue dotted line), and ISIS VESUVIO [8] (dash-dotted line). The reference terrestrial neutron flux data [4], multiplied by 3×10^9, are represented by a black thick solid line. (*b*) The same data on a "lethargy plot".

The ANITA-CUP spectral flux in the lethargy representation (Figs. 5b and 8b) is dominated by two broad peaks at ~1 MeV and ~80 MeV, which can be attributed to two different neutron emission mechanisms in nuclear reactions. The high-energy peak is due to neutrons emitted at the primary, or *cascade*, stage of the reaction, whereas the low-energy peak comes from nucleon *evaporation* processes at later stages of de-excitation. The peaks in the reference terrestrial spectrum [4] are located approximately at the same energies. On the other hand, the evaporation peak at ~0.5-10 MeV is more pronounced in the ANITA-CUP spectrum relative to the terrestrial one and to e.g. the spectrum at LANSCE ICE House. Consequently, for devices with SEE thresholds below 10 MeV, FIT rate measurements at the CUP may give overestimated results, which can be corrected following the method suggested by Platt *et al* [31] that would make use of the quasi-monoenergetic neutron (QMN) option [32], with proton beam incident on a thin ^{7}Li target (see Fig. 1), and/or a similar method that would utilize the possibility to modulate the CUP spectrum by using different collimator apertures (see Fig. 4). Development of those options, as well as deeper comparisons with the other facilities, goes beyond the scope and the volume limitations of the present paper. Concerning the high-energy end of the spectrum, the ANITA-CUP facility is capable of revealing SEE for DUTs with thresholds up to ~150 MeV.

VI. Features of the CUP Facility

In Table III we summarize the maximum overall dimensions of the DUT that can be accommodated at the CUP. Dependent on the overall thickness of the DUT (i.e., the thickness of the PCB together with the maximum height of the components), one of the two geometrical options are available for the user.

Table III.
The Maximum Overall Dimensions of the DUT at the CUP

Option #	Thickness (mm)	Width (mm)	Height (mm) that can be accommodated in the trolley sled	Height (mm) that can be accommodated in the beam
1	45	180	500	200
2	25	204		

The trolley sled can accommodate a DUT with the height up to 50 cm, whereas only a 20-cm high part of the device can be irradiated at once. The height of the trolley sled is adjusted to the actual height of the DUT in such a way that the beam spot is centered on the DUT. The maximum weight of the DUT is 1.5 kg. The DUT is put on the trolley sled, using the mounting trenches at both the upper and the lower parts of the sled. The trenches can accommodate a 2-mm thick PCB bearing the DUT. Other thicknesses can be accommodated by prior request. The space available at the CUP should be sufficient for testing of electronic components and smaller-scale systems. Users' peripheral equipment can be installed out-of-beam, near the access shaft.

The DUT may get radioactive during the irradiation, and may remain radioactive for a period of time afterwards. The same applies for CUP surroundings. Enhanced dose rate levels may show up also in the proximity of the access shaft, located at a restricted area with continuous dose rate monitoring.

VII. Conclusions and Outlook

The ANITA-CUP neutron facility with atmospheric-like spectrum has been characterized and put into operation for nSER testing. The characterization measurements have confirmed the availability of the neutron flux that is currently the highest among the facilities in the same class. CUP should be particularly attractive for testing of devices that include high-Z materials, e.g., tungsten, since their presence near sensitive volumes may lead to increased radiation sensitivity [33], attributed to densely-ionizing fragments originating from

high-energy neutron-induced fission of high-Z materials [12].

The developed multicomponent model has been found useful for realistic description and understanding of the neutron field in the CUP area. The employed characterization and simulation techniques are generally applicable for a broad class of neutron irradiation facilities. Detection techniques based on neutron-induced fission reactions provide a powerful tool for spectral fluence measurements, especially if a few target nuclides are involved and/or the facility is ToF-capable. The measurement results function as a test of model calculations, which become increasingly detailed and affordable due to the unprecedented development of computational power.

ACKNOWLEDGMENT

The CUP development was stimulated by requests from S.-J. Wen, B. Bhuva, R. Edwards, A. Wallner, and T. Nuns. The authors wish to thank G. Gorini, R. Nolte, N. Olsson, A. Paccagnella, S. P. Platt, M. Romain, A. N. Smirnov, and R. Wong for valuable discussions, O. Jonsson for prototyping, S. Holm for the final technical design, C. Allabush and N. Gaspard for participation in pilot runs. We thank C.-J. Fridén, B. Gålnander, T. Johansen, D. Lundgren, L. Pettersson, and the staff of TSL for participation in the development and commissioning of the new facility.

REFERENCES

[1] J. F. Ziegler and H. Puchner, SER – *History, Trends and Challenges*. Cypress Semiconductor, 2004.

[2] T. Nakamura, M. Baba, E. Ibe, Y. Yahagi, and H. Kameyama, *Terrestrial Neutron-Induced Soft Errors in Advanced Memory Devices*, 1st ed., Singapore, World Scientific, 2008.

[3] N. Kanekawa, E. H. Ibe, T. Suga, and Y. Uematsu, "Terrestrial neutron-induced failures in semiconductor devices and relevant systems and their mitigation techniques," in *Dependability in Electronic Systems*, Springer, 2011.

[4] *Measurement and Reporting of Alpha Particle and Terrestrial Cosmic Ray-Induced Soft Errors in Semiconductor Devices*, JEDEC Standard JESD89A, 2006.

[5] *Process Management for Avionics – Atmospheric Radiation Effects – Part 2: Guidelines for single event effects testing for avionics systems*, IEC International Standard 62396-2, 2012.

[6] The ICE House, Los Alamos Neutron Science Center. Available: http://lansce.lanl.gov/NS/instruments/ICEhouse/

[7] E. W. Blackmore, P. E. Dodd, and M. R. Shaneyfelt, "Improved capabilities for proton and neutron irradiations at TRIUMF", *IEEE Radiation Effects Data Workshop*, Monterey, CA, 2003, pp. 149-155.

[8] C. Andreani, A. Pietropaolo, A. Salsano, G. Gorini, M. Tardocchi, A. Paccagnella, S. Gerardin, C. D. Frost, S. Ansell, and S. P. Platt, "Facility for fast neutron irradiation tests of electronics at the ISIS spallation neutron source", *Appl. Phys. Lett.*, vol. 92, p. 114101 (2008).

[9] A. V. Prokofiev, J. Blomgren, M. Majerle, R. Nolte, S. Röttger, S. P. Platt, X. X. Cai, and A. N. Smirnov, "Characterization of the ANITA neutron source for accelerated SEE Testing at The Svedberg Laboratory", *IEEE Radiation Effects Data Workshop*, Quebec, Canada, 2009, pp. 166-173.

[10] V. P. Eismont, A. V. Prokofiev, and A. N. Smirnov, "Thin film breakdown counters and their applications (review)", *Radiat. Meas.*, vol. 25, pp. 151-156, 1995.

[11] A. N. Smirnov, A. Pietropaolo, A. V. Prokofiev, E. E. Rodionova, C. D. Frost, S. Ansell, E. M. Schooneveld, and G. Gorini, "Application of thin-film breakdown counters for characterization of neutron field of the VESUVIO instrument at the ISIS spallation source", *Nuclear Instruments and Methods in Phys. Res.*, vol. A687, pp. 14-22, 2012.

[12] A. N. Smirnov, V. P. Eismont, N. P. Filatov, J. Blomgren, H. Condé, A. V. Prokofiev, P.-U. Renberg, and N. Olsson, "Measurements of neutron-induced fission cross-sections for ^{209}Bi, ^{nat}Pb, ^{208}Pb, ^{197}Au, ^{nat}W, and ^{181}Ta in the intermediate energy region", *Phys. Rev.*, vol. C70, p. 054603, 2004.

[13] N. B. Patel and H. Puchner, "Correlation of soft error rates between mono-energetic and full spectrum beams on a 90nm SRAM technology", in *Proc. IEEE International Reliability Physics Symposium*, Montreal, Canada, 2009, pp. 948–951.

[14] S. Gerardin, M. Bagatin, A. Paccagnella, G. Cellere, A. Visconti, M. Bonanomi, A. Hjalmarsson, and A. V. Prokofiev, "Heavy-ion induced threshold voltage tails in floating gate arrays", *IEEE Trans. Nucl. Sci.*, vol. 57, pp. 3199-3205, 2010.

[15] Y. Chen, "Cosmic ray effects on cellphone, laptop, and USB flash drive applications", presented at the 9th Workshop on Silicon Errors in Logic - System Effects (SELSE-9), Stanford University, CA, March 26-27, 2013.

[16] N. Gaspard *et al.*, "Estimation of hardened flip-flop neutron soft error rates using SRAM multiple-cell upset data in bulk CMOS", in *Proc. IEEE International Reliability Physics Symposium*, Anaheim, CA, 2013, pp. SE.6.1 – SE.6.5.

[17] G. G. Nampoothiri, M. L. R. Horemans, A. J. P. Theuwissen, "Ageing effects on image sensors due to terrestrial cosmic radiation", in *Proc. SPIE* 7875, *Sensors, Cameras, and Systems for Industrial, Scientific, and Consumer Applications XII*, 78750G (February 16, 2011).

[18] A. Hands and C. Dyer, "A technique for measuring dose equivalent and neutron fluxes in radiation environments using silicon diodes", *IEEE Trans. Nucl. Sci.*, vol. 56, pp. 3442–3449, 2009.

[19] V. Lacoste, "Review of radiation sources, calibration facilities and simulated workplace fields", *Radiation Measurements*, vol. 45, pp. 1083-1089, 2010.

[20] Xiao Xiao Cai and S. P. Platt, "Modeling neutron interactions and charge collection in the imaging single-event effects monitor", *IEEE Trans. Nucl. Sci.*, vol. 58, no. 3, pp. 910-915, June 2011.

[21] L. H. Zhang, S. P. Platt, R. H. Edwards, and C. Allabush, "In-situ neutron dosimetry for single-event effect accelerated testing", *IEEE Trans. Nucl. Sci.*, vol. 56, no. 4, pp. 2070-2076, August 2009.

[22] F. Wrobel *et al.*, "A silicon diode-based detector for investigations of atmospheric radiation", *IEEE Trans. Nucl. Sci.*, vol. 60, no. 5, pp. 3603-3608, October 2013.

[23] MCNPX User's Manual, Version 2.3.0, LA-UR-02-2607, April 2002.

[24] The MCNPX code, Los Alamos National Laboratory. Available: http://mcnpx.lanl.gov

[25] M.B. Chadwick, *et al.*, "Cross-section evaluations to 150 MeV for accelerator-driven systems and implementation in MCNPX", *Nuclear Science and Engineering*, vol. 131, no. 3, pp. 293-328, 1999.

[26] S. G. Mashnik, K. K. Gudima, R. E. Prael, A. J. Sierk, M. I. Baznat, and N. V. Mokhov, "CEM03.03 and LAQGSM03.03 event generators for the MCNP6, MCNPX, and MARS15 transport codes", LA-UR-08-2931, presented at Advanced Workshop on Model Codes for Spallation Reactions, ICTP, Trieste, Italy, February 4 - 8, 2008.

[27] A. D. Carlson, S. Chiba, F.-J. Hambsch, N. Olsson, and A. N. Smirnov, "Update to nuclear data standards for nuclear measurements", in Proc. Int. Conf. Nuclear Data for Science and Technology, Trieste, Italy, 1997, Italian Physical Society Conference Proceedings, vol. 59, Part II, pp. 1223-1229.

[28] *Standard Practice for Characterizing Neutron Energy Fluence Spectra in Terms of an Equivalent Monoenergetic Neutron Fluence for Radiation-Hardness Testing of Electronics*, ASTM Standard E722, 2007.

[29] A. Vasilescu and G. Lindström, "Displacement damage in Silicon". [Online]. Available: www.researchgate.net/publication/234719569_neutrons

[30] R. Baumann and E. B. Smith, "Neutron-induced ^{10}B fission as a major source of soft errors in high density SRAMs", *Microelectronics Reliability*, vol. 41, no. 2, pp. 211-218, Feb. 2001.

[31] S.P. Platt, A.V. Prokofiev, X.X. Cai, "Fidelity of energy spectra at neutron facilities for single-event effects testing", Proc. 2010 IEEE International Reliability Physics Symposium (IRPS), pp. 411–416.

[32] A. V. Prokofiev, J. Blomgren, O. Byström, C. Ekström, S. Pomp, U. Tippawan, V. Ziemann, and M. Österlund, "The TSL neutron beam facility", *Rad. Prot. Dosim.*, vol. 126, pp. 18-22, 2007.

[33] M. A. Clemens, *et al.*, "The effects of neutron energy and high-Z materials on single event upsets and multiple cell upsets", *IEEE Trans. Nucl. Sci.*, vol. 58, pp. 2591–2598, 2011.